AD

MEMORANDUM REPORT ARBRL-MR-03135

MEASUREMENT PROBLEMS IN HIGH VELOCITY IMPACT EXPERIMENTS

William Lawrence

September 1981

US ARMY ARMAMENT RESEARCH AND DEVELOPMENT COMMAND
BALLISTIC RESEARCH LABORATORY
ABERDEEN PROVING GROUND, MARYLAND

Destroy this report when it is no longer needed.
Do not return it to the originator.

Secondary distribution of this report by originating or sponsoring activity is prohibited.

Additional copies of this report may be obtained from the National Technical Information Service, U.S. Department of Commerce, Springfield, Virginia 22151.

The findings in this report are not to be construed as an official Department of the Army position, unless so designated by other authorized documents.

The use of trade names or manufacturers' names in this report does not constitute indorsement of any commercial product.

UNCLASSIFIED

SECURITY CLASSIFICATION OF THIS PAGE (When Data Entered)

REPORT DOCUMENTATION PAGE	READ INSTRUCTIONS BEFORE COMPLETING FORM
1. REPORT NUMBER: Memorandum Report ARBRL-MR-03135	2. GOVT ACCESSION NO. / 3. RECIPIENT'S CATALOG NUMBER
4. TITLE (and Subtitle): Measurement Problems in High Velocity Impact Experiments.	5. TYPE OF REPORT & PERIOD COVERED: Final
	6. PERFORMING ORG. REPORT NUMBER
7. AUTHOR(s): William Lawrence	8. CONTRACT OR GRANT NUMBER(s)
9. PERFORMING ORGANIZATION NAME AND ADDRESS: US Army Ballistic Research Laboratory, Aberdeen Proving Ground, MD 21005	10. PROGRAM ELEMENT, PROJECT, TASK AREA & WORK UNIT NUMBERS: 1L161102AH43
11. CONTROLLING OFFICE NAME AND ADDRESS: USA Armament Research and Development Command, USA Ballistic Research Laboratory (DRDAR-BL), Aberdeen Proving Ground, MD 21005	12. REPORT DATE: SEPTEMBER 1981
	13. NUMBER OF PAGES: 38
14. MONITORING AGENCY NAME & ADDRESS (if different from Controlling Office)	15. SECURITY CLASS. (of this report): Unclassified
	15a. DECLASSIFICATION/DOWNGRADING SCHEDULE

16. DISTRIBUTION STATEMENT (of this Report)

Approved for public release; distribution unlimited.

17. DISTRIBUTION STATEMENT (of the abstract entered in Block 20, if different from Report)

18. SUPPLEMENTARY NOTES

19. KEY WORDS (Continue on reverse side if necessary and identify by block number)

Long-rod projectile, Ballistics, Penetration velocity, Rolled homogeneous armor, Strain gages, Optical distortion.

20. ABSTRACT (Continue on reverse side if necessary and identify by block number) bet/2972

Reverse-ballistic experiments have been performed at the Ballistic Research Laboratory using a light-gas gun to launch targets against stationary long-rod projectiles instrumented with foil type resistance strain gages. Signals from the strain gages are recorded, measured and analyzed to obtain information about the dynamic behavior of the projectile as it penetrates the target. Signals from the strain gages are commonly divided so that part of the signal may be displayed at higher amplification for better resolution of detail at

DD FORM 1 JAN 73 1473 EDITION OF 1 NOV 65 IS OBSOLETE

UNCLASSIFIED

SECURITY CLASSIFICATION OF THIS PAGE (When Data Entered)

low strains. Data recorded at different deflection sensitivities and data from gages at diametrically opposed locations on the projectiles are combined for the analysis. Error in the data reduction, especially error in time, is apparent from the poor agreement of the combined data. Different sources of error have been identified but the primary source is optical distortion in the oscilloscope cameras and in the copying camera. This report briefly reviews the instrumented rod experiment and the analytical procedure but primarily considers sources of error. A modified calibration procedure is introduced to minimize the error in the data reduction.

TABLE OF CONTENTS

LIST OF ILLUSTRATIONS

I. INTRODUCTION

Reverse-ballistic experiments have been performed at the Ballistic Research Laboratory using a light-gas gun to launch targets against stationary long-rod projectiles instrumented with foil-type resistance strain gages. Signals from the strain gages are recorded, measured and analyzed to obtain information about the dynamic behavior of the projectile as it penetrates the target. Signals have been displayed by cathode-ray oscilloscopes and recorded photographically. The nature of stress-wave propagation in long-rod projectiles has necessitated long observation times and simultaneous observation of each signal at different deflection sensitivities in order to achieve acceptable resolution at both high and low strain levels. Data recorded at different deflection sensitivities and data from gages at diametrically opposed locations on the projectile must be combined for the analysis. Error in the data reduction, especially error in time, is apparent from the poor agreement of the combined data. Different sources of error have been identified but the primary source is optical distortion in the oscilloscope cameras and in the copying camera which produces a transparency from the original photographic polaroid record. Strain-gage signals recorded early in the investigation were especially susceptible to error from optical distortion; refined procedures in later experiments reduced the error but did not eliminate it. This report briefly reviews the instrumented-rod experiment and the analytical procedure, but primarily considers sources of error.

II. BACKGROUND

The general nature of the experimental approach will be reviewed before problem areas are introduced. This section briefly describes the experiments, the reduction of data, and the analytical procedure. Greater experimental detail has been reported by Hauver and Melani[1], while the theoretical basis for the analysis has been reported by Wright[2].

A. Experimentation.

Reverse-ballistic experiments have been performed at the Ballistic Research Laboratory using a 100 mm light-gas gun to impact targets against stationary long-rod penetrators instrumented with foil strain-gages. The experimental arrangement of a reverse-ballistic experiment at 710 m/s is shown in Figure 1. A long steel rod is shown instrumented with pairs of strain gages which are located 20, 40, 60, and 80 mm from the tip of the rod. This rod is impacted at normal incidence by a plate of rolled

---

[1] *G. E. Hauver, "Penetration with Instrumented Rods," Int. J. Eng. Sci., 16, pp. (871-877), 1978.*

[2] *T. W. Wright, "A Theoretical Framework and Comparison with Instrumented Impacts," 12th Annual Army Science Conference, West Point, NY, 1980.*

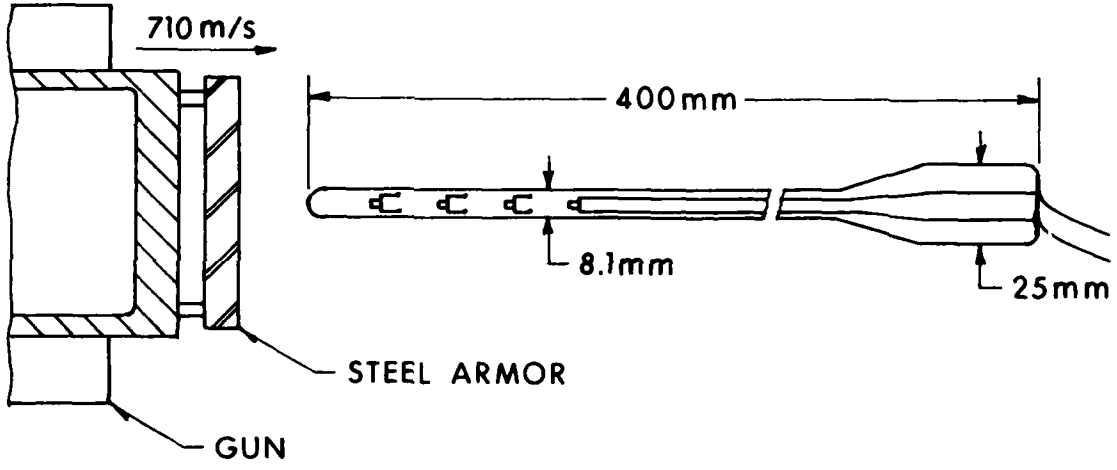

Figure 1. Experimental Arrangement of Normal Impact in Reverse-Ballistic

homogeneous armor launched from the gun. A compression wave travels back the rod and is detected by changes in gage resistance. These changes in resistance are measured by bridge circuits, and the output signal from each bridge is displayed by a cathode-ray oscilloscope and recorded photographically on Polaroid type 410 film. Signals from the strain gages are commonly divided so that part of the signal may be displayed at higher amplification for better resolution of detail at low strains. Divided signals from a strain gage in an early experiment are shown in Figure 2. With diametrically opposed gages at each rod location, and each signal divided, four sets of data must be reduced and combined to provide a single strain-time history at each location on the rod. These combined strain-time plots are shown in Figure 3.

Oscilloscopes are calibrated by substituting a strain gage which is similar to those on the rod. This procedure reduces the danger of damaging or destroying a test gage prior to the impact experiment. Calibration consists of triggering the bridge circuit and measuring the resistance with several different precision resistors in parallel with the gage. This calibration establishes a constant which, together with the circuit constants, relates oscilloscope deflection to resistance change. Before applying this calibration to reduce test data, the circuit constants are re-evaluated using the correct resistances for gages on the rod and corrected balance points for the bridges.

B. Data Reduction and Analysis.

The original records on Polaroid Type 410 film are copied onto Polaroid Type 146-L film to obtain transparencies which are measured on an optical comparator that provides a digital X-Y output. These X-Y coordinates are converted to time and strain respectively, using calibration and reference points on both axes. Time, t, has been determined from the expression,

$$t = a+bX+cX^2+dX^3$$

where a, b, c, and d are coefficients from a least-square cubic fit to reference time marks. Strain, ε, is determined from the expression,

$$\varepsilon - \varepsilon_o = \frac{\left(C_1/FGR_G\right)\left(Y-Y_o\right)}{\left(1- C_2/F\right)\left(Y-Y_o\right)}$$

where R_G is the initial resistance of the strain gage, C_1 and C_2 are Constants which depend on resistances in the bridge circuit[1], G is the strain-gage factor, and F is the calibration factor. Since the rod is initially unstrained and the bridge is initially balanced, $\varepsilon_o = 0$. The gage factor, G, is assumed to be $(2+\varepsilon)$; this assumption has been verified

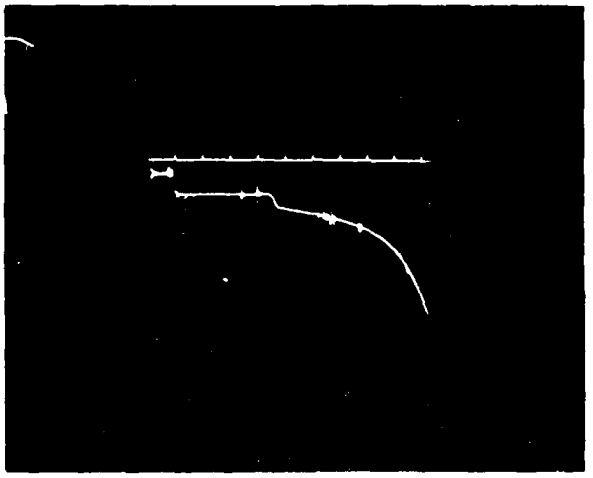

A 5%

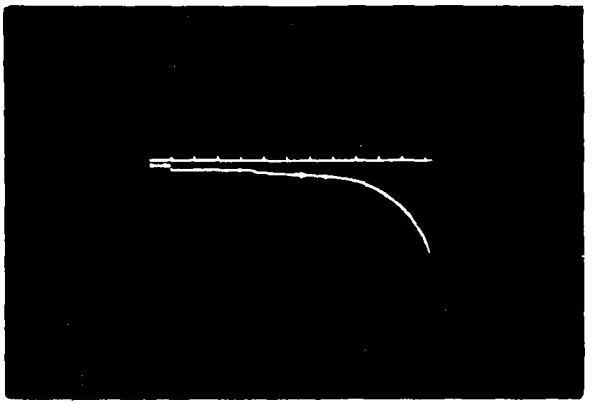

B 20%

Figure 7. Divided Signals at 5% and 20% Strain

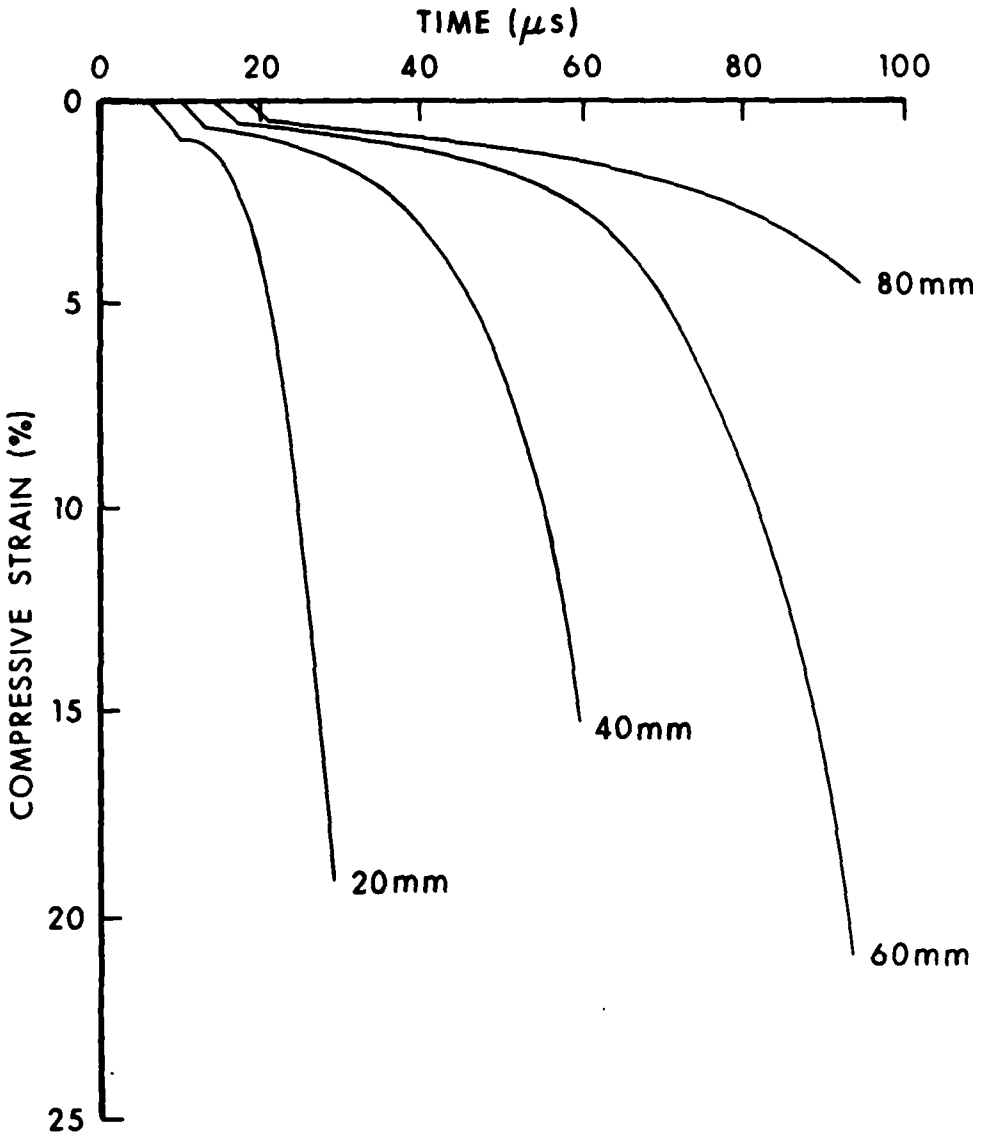

Figure 3. Combined Strain-Time Plots at Different Locations

by quasi-static experiments reported by Franz[3]. The calibration factor, F, is determined from the expression,

$$F = \frac{Y-Y_o}{\Delta R'} \left(C_1'+C_2'\Delta R'\right) ,$$

where primes refer specifically to the calibration. C_1' and C_2' again are the circuit constants, and $\Delta R'$ is given by the expression

$$\Delta R' = R_g' \left(\frac{R_c}{R_c - R_g'} - 1 \right)$$

where R_c is the resistance of the calibrating resistor, and R_g' is the resistance of the strain gage substituted for calibration.

This procedure for data reduction provides four strain-time histories at each location on the long-rod penetrator. These data are then combined to provide single strain-time history at each location.

C. Analytical Procedure.

The strain-time histories from different locations on the rod are used to perform a simple wave analysis. From the strain time histories, curves for constant strain may be plotted in distance-time space. Along these curves the slope is defined as C_p, the plastic wave velocity. In the strain-time histories for steel penetrators, these curves have been straight lines indicating that the wave speed is independent of strain rate. These plots are shown in Figure 4. A plot of wave velocity vs. strain is prepared, and a representative plot is shown in Figure 5. Based on the strain-rate independent theory for plastic wave propagation, particle velocity and stress are determined from the expressions:

$$U = \int_o^\varepsilon C_p \, d\varepsilon ,$$

and,

$$\sigma = \int_o^\varepsilon \rho \, C_p^{\,2} \, d\varepsilon$$

---

[3]*R. E. Franz, "Quasi-Static Stress-Strain Curves, S-7 Tool Steel," Report No. ARBRL-MR-03067, Ballistic Research Laboratory, Aberdeen Proving Ground, MD.* (AD #A093773)

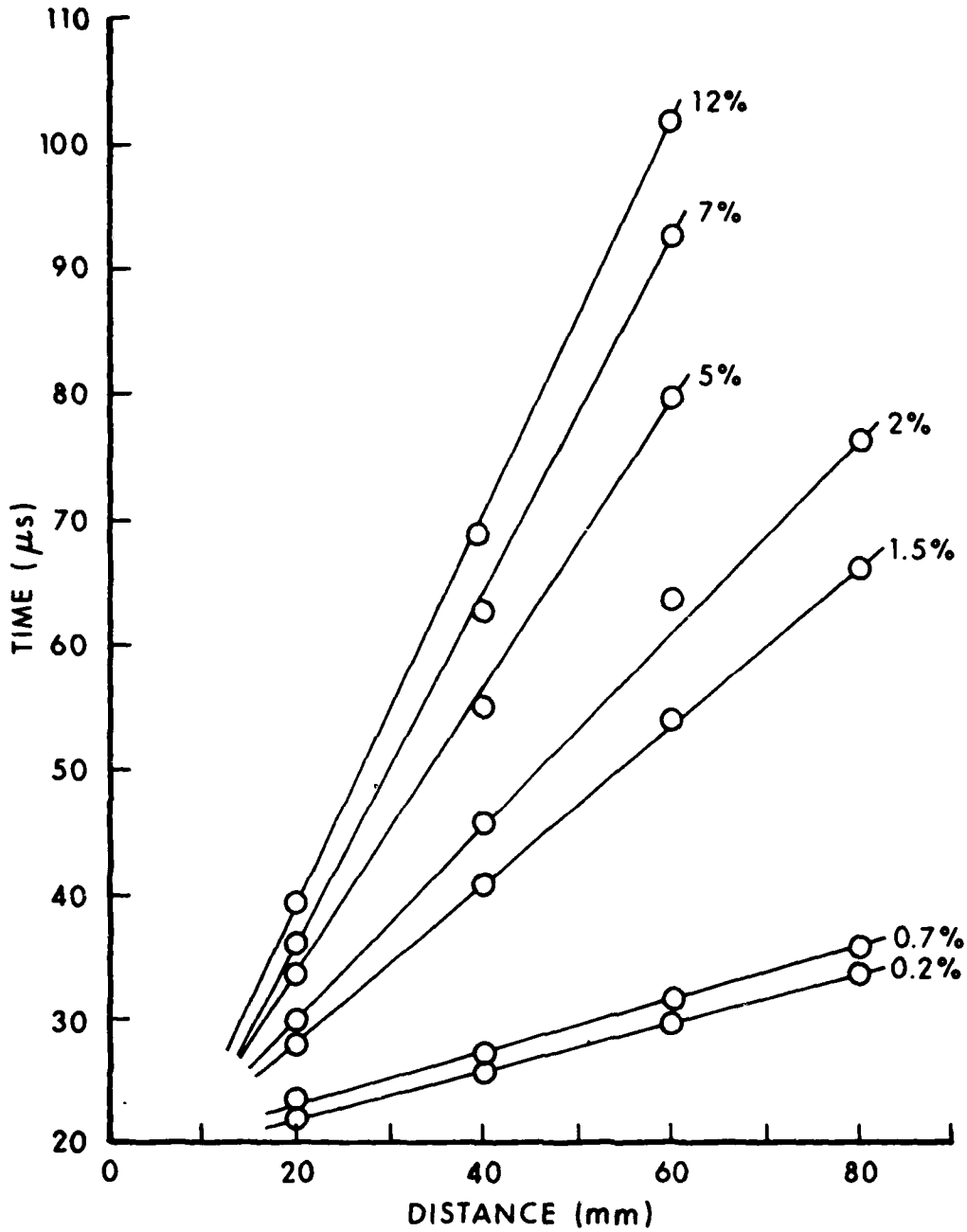

Figure 4. Distance-Time Plots

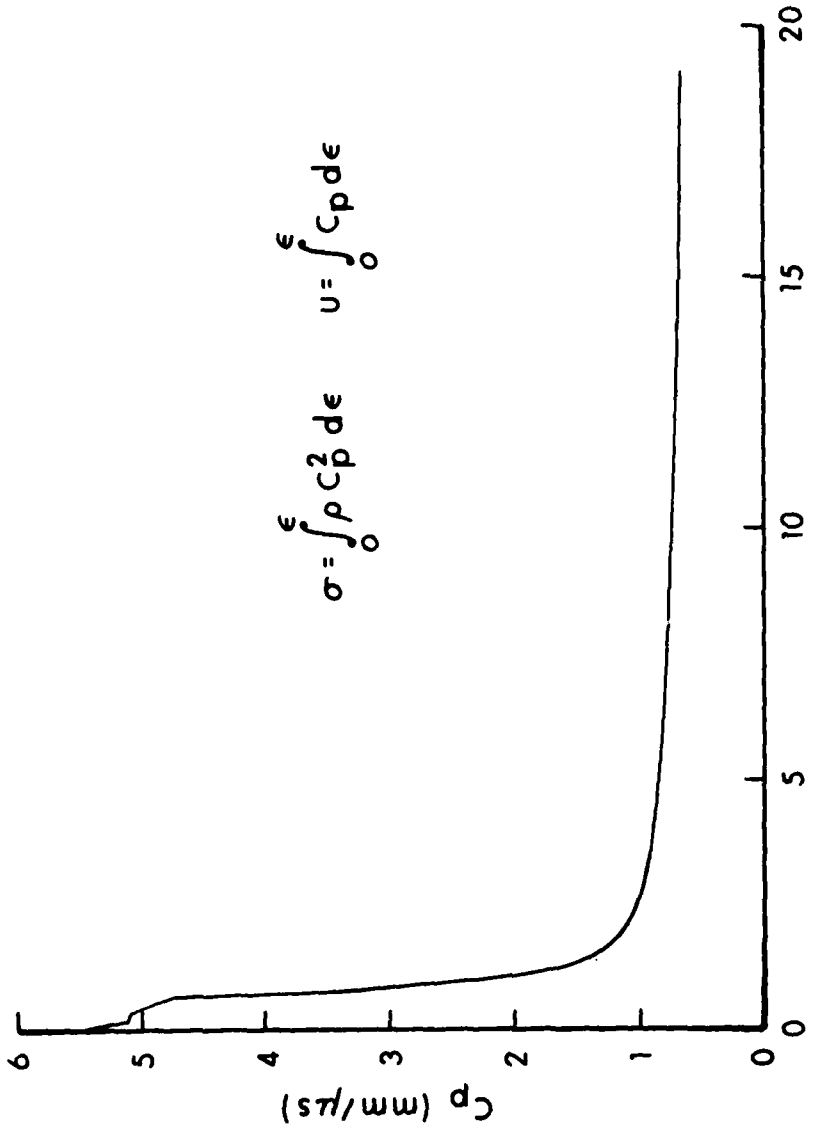

Figure 5. Wave Velocity-Strain Plot

where U is the particle velocity, σ is the stress, and ρ is the density. Stress-strain and particle velocity - strain plots are shown in Figure 6. The theoretical basis for investigation of instrumented penetrators is reported in Reference 2.

III. PROBLEMS AND DISCUSSION

Figure 3 shows strain-time histories measured at four gage locations on a long-rod penetrator. Problems associated with the measurement and analysis of oscilloscope records become evident when the details of Figure 3 are considered. The high levels of strain travel relatively slowly and a minimum recording time of at least 100 μs is required to record the arrival of high strain levels at a gage located only 60 mm from the tip of the rod. Arrivals of the elastic front at each gage location are then crowded into a short time interval because an elastic wave travels at a velocity which may be nearly ten times the velocity of a plastic wave at a higher strain level of about 15 percent. This short time interval imposes a requirement for highly accurate time measurements in order to establish the elastic-wave velocity with acceptable accuracy. Measurements of signal amplitude encounter a similar problem. Strain in the elastic region is usually limited to values below one percent, while strain in the plastic region can frequently be measured to values exceeding twenty percent. In principle, the accuracy with which time and amplitude are measured can be improved by dividing signals and simultaneously recording them at different sweep rates and different amplifications. In practice, this would require many recording channels and, for economic considerations at this laboratory, signals are divided only to record at different amplifications for better resolution of strain in the elastic and low-plastic regions. Divided signals from gages at the same location on both sides of the rod must be measured and combined for an analysis. These measured signals are commonly displaced from each other as shown in Table I and cannot be combined without arbitrary adjustments; these displacements provide evidence of measurment error.

In an effort to use the data from tests already performed, a procedure for combining test data was developed. At each rod location the four sets of strain-time data were forced into agreement at the mean arrival time for the midpoint of the elastic fronts. It was next assumed that the more highly amplified records provided a more accurate measurement of strain, and these two records were adjusted slightly for closest agreement in the region of low-plastic strain. This adjustment was achieved by equal but opposite changes in respective values of the deflection factor, F. The less amplified measurements of high strain were assumed to be less accurate and the deflection factor, F, for each set of data was adjusted to produce agreement at the upper limit of low-strain data. After combining data at each rod location, a distance-time diagram was prepared as the first step in the analysis. A distance-time diagram is shown in Figure 4. The data in these distance-time diagrams exhibited significant scatter which suggested that the procedure

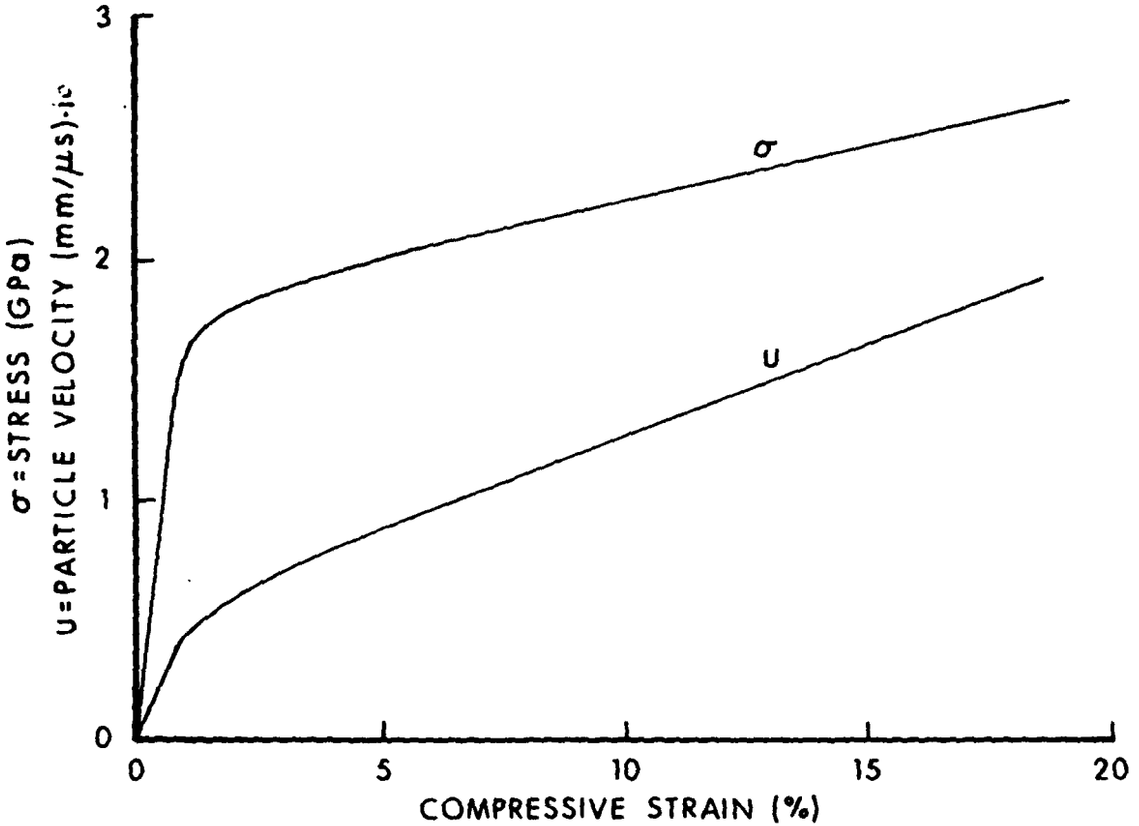

Figure 6. Stress-Strain and Particle Velocity-Strain Plots

TABLE I

WAVE ARRIVAL TIME AT DIFFERENT LOCATIONS

GAGE NO.	ε(%)	LOCATION	ARRIVAL TIME (μs)	TIME DIFF (μs)
4	5	20mm	21.665	0.614
	20		21.051	
5	5		—	
	20		21.593	
3	5	40mm	24.511	0.467
	20		24.217	
6	5		24.249	
	20		24.044	
2	5	60mm	28.368	1.028
	20		27.340	
7	5		28.008	
	20		27.680	
1	5	80mm	31.426	0.108
8	5		31.318	

developed to combine data did not overcome the measurement errors. Consequently, tests were performed to learn more about the sources of measurement error and to find a way to reduce their influence on results.

Before examining sources of error it should be noted that the errors in strain or time to be considered result primarily from errors in measurements of distance on photographic records. It will also be useful to consider the magnitude of error which is a concern. Measurements in the strain direction are relatively insensitive to measurement error if one-percent accuracy is required. In practice the signals are divided and recorded at different amplifications. Typical dimensions on the two calibration records are 16 mm equals five percent strain and twenty percent strain, respectively; one percent accuracy requires that distance be determined within ±.16 mm (0.0063 inch). One-percent accuracy is not considered an unreasonable goal in strain measurements; however, this goal can be more difficult to achieve in time measurements. On a typical photographic record a distance of 40 mm may correspond to a time interval of 150 μs. If the time interval between the arrival of a high strain level at two gage locations is 70 μs, the film distance must be measured within 0.19 mm (.0075 inch) for one-percent accuracy. However, if the time interval is only 10 μs, as it may be at the elastic front, the film distance must be determined within approximately 0.027 mm (.0011 inch) for one-percent accuracy, and this measurement is more demanding. Although these considerations are not exact, they nevertheless provide a general guide to the requirements for accuracy.

Errors in the measurement of time influence the accuracy of wave velocities and consequently the accuracy of analytical results. Wave velocity, determined from measurements of arrival time at known strain-gage locations on a long-rod penetrator, is plotted as a function of strain in Figure 5. Integrations along this curve yield the relationships between stress and strain and between particle velocity and strain. The large area under the initial portion of the curve in Figure 5 is very influential in the integrations. Unfortunately, the high wave velocities at the beginning of the curve are less reliable because of errors in the measurement of arrival time.

Measurement errors can arise from different sources. The major sources are believed to be optical distortion, film distortion, and mechanical alignment of the camera. Errors also relate to image quality and the ability of a human operator to read and interpret images correctly[4]. Additional error may also be introduced by the comparator used for record measurements. Each of these sources of error has been considered and will be discussed in the following sections.

---

[4] *D. D. Preonas and R. F. Prater, "Quantitative Motion Analysis from Rotating Mirror Framing Camera Records," Journal of the SMPTE, Vol. 79, July 1970.*

A. Optical Distortion.

Optical distortion introduced by the oscilloscope and copying cameras was determined by measuring photographs of a precision glass grid. Distortion plots such as the one shown in Figure 7 were prepared from these measurements. The distortion in these plots was exaggerated by measuring the displacement between the intersection points on the photograph and corresponding intersection points on the precision grid, multiplying this displacement by a factor of 1000, and plotting this magnified displacement on the scale of the precision grid. Figure 7 shows distortion produced by an oscilloscope camera. Similar negative distortion is produced by the Polaroid MP-4 camera which has been used to produce a transparent copy of the original record. Consequently, a test record such as shown in Figure 7 contains distortion similar to that in Figure 2-A, and producing a transparent copy would increase the distortion. This scale does not apply to solid line.

The source of measurement error becomes evident when the measurement procedure is reviewed. First, the record must be aligned on the stage of the measuring instrument. In Figure 2-A the reference sweep with superimposed time marks is located near the upper extreme of the distorted grid in Figure 7. The operator discovers that the reference sweep is curved, must decide which portion of the sweep should be used for alignment, and probably chooses to align over the central region adjacent to the beginning and early portion of the signal. Then, assuming the distortion shown in Figure 7, as the signal amplitude increases (negatively in Figure 2-A), the orthogonal motions of the measuring instrument will yield times which are too late and time intervals (relative to the beginning of the signal) which are too long. For a record similar to that shown in Figure 2-A, it is estimated that timing error of 0.3 μs or more could occur, and would depend upon the specific location of the signal and choices made by the operator.

B. Film Distortion.

Film distortion is a factor which limits the accuracy of a measurement, and it is difficult to eliminate. The primary causes of distortion are dimensional changes of the film base which undergoes various temporary and permanent changes between exposure to the image and measurement of the processed record.[5] Experimental study of oscilloscope records has revealed measurable distortion which results from lack of film flatness. When the record is removed from the camera it curls during the drying process. Then, when the record is flattened for a measurement, the emulsion stretches introducing elongation of an image already distorted. This elongation was detected when a precision glass grid was photographed on both Polaroid-Type 410 film and Polaroid Type 146-L film. The Type 410 film curled much less than the Type 146-L film.

---

[5] *J. Vlcek, "Systematic Errors of Image Coordinates," Photogrammetric Engineering, Vol. 35, pp. 585-593, 1969.*

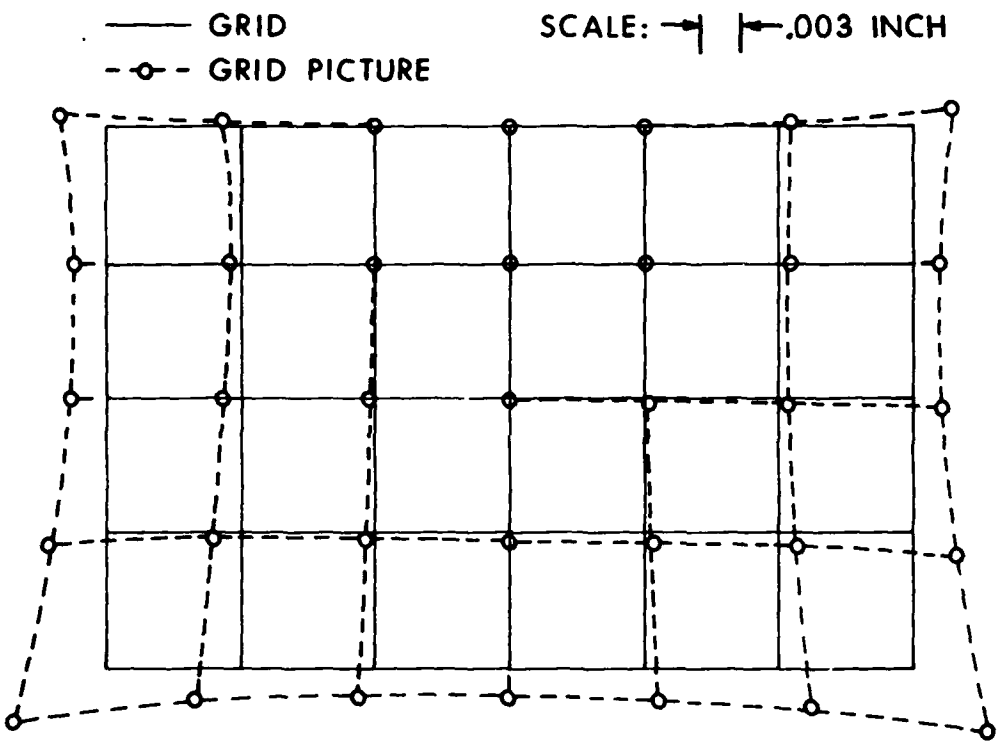

Figure 7. Asymmetry because of Camera, and Distortion Plot

Figure 8 shows that distortion produced by the Type 410 film was more symmetrical than distortion produced by the Type 146-L film, and this result is consistent with the observation about curl. Although the distortion produced by the Type 410 film is more symmetrical, it is also somewhat greater than the distortion of Type 146-L film, as may be observed at the top and bottom of Figure 8. This suggests that the paper base of the Type 410 film may be dimensionally less stable than the plastic base of Type 146-L film. Vlcek[5] made a compensation for film distortion by employing four simulated corner fiducial marks and found that errors larger than 0.01 mm were quite common. Although it is difficult to separate film distortion from optical distortion, the 0.01 mm value is judged to be reasonably consistent with the film distortion evident in Figure 8. This scale does not apply to solid line.

C. Camera Stability.

Mechanical characteristics may also contribute to measurement error. These cameras may not be rigidly constructed and exact alignment may be difficult to maintain. There is a tendency for cameras to droop, and there may be a considerable amount of movement in the assembly that attaches the camera to the oscilloscope. If the camera is opened or removed to reposition the cathode-ray beam, care must be taken to prevent misalignment. The adapter that attaches the camera to the oscilloscope may allow motion of approximately 0.05 mm. When a camera droops, it pivots around its lower point of support on the oscilloscope, leaving a gap of 0.5 mm at the top. Drooping therefore moves the camera away from the face of the cathode ray tube. With the image distance fixed, this movement increases the object distance and decreases the magnification slightly. By calculation, the length of the lower half of the image decreases by 0.0305 mm while the upper half of the image decreases by 0.0096 mm. The difference of approximately 0.02 mm accounts just under one-half the observed asymmetry in the distortion plot. The remaining asymmetry is assumed to result from elastic yielding of the camera assembly. It has been shown that lifting the camera to reverse the influence of droop almost exactly reverses the asymmetry of the distortion plot and shows that the asymmetry results from mechanical misalignment of the camera. Poor camera rigidity can conceivably introduce asymmetry into the distortion as shown in Figure 7 where the distortion is obviously greater at the bottom of the record than at the top. Accurate alignment of the Polaroid MP-4 Copier is also difficult to achieve and maintain, especially if the instrument is used and adjusted by different operators.

D. Common Reference Error.

Data reduction and analysis require a reference point in time which is common to all test records. A common time reference has been introduced in different ways, but the most successful reference prior to impact has been provided either by briefly blanking the cathode-ray beam or by superimposing a brief RC discharge signal. With beam blanking, the point where the beam begins to narrow or round just before it disappears, serves

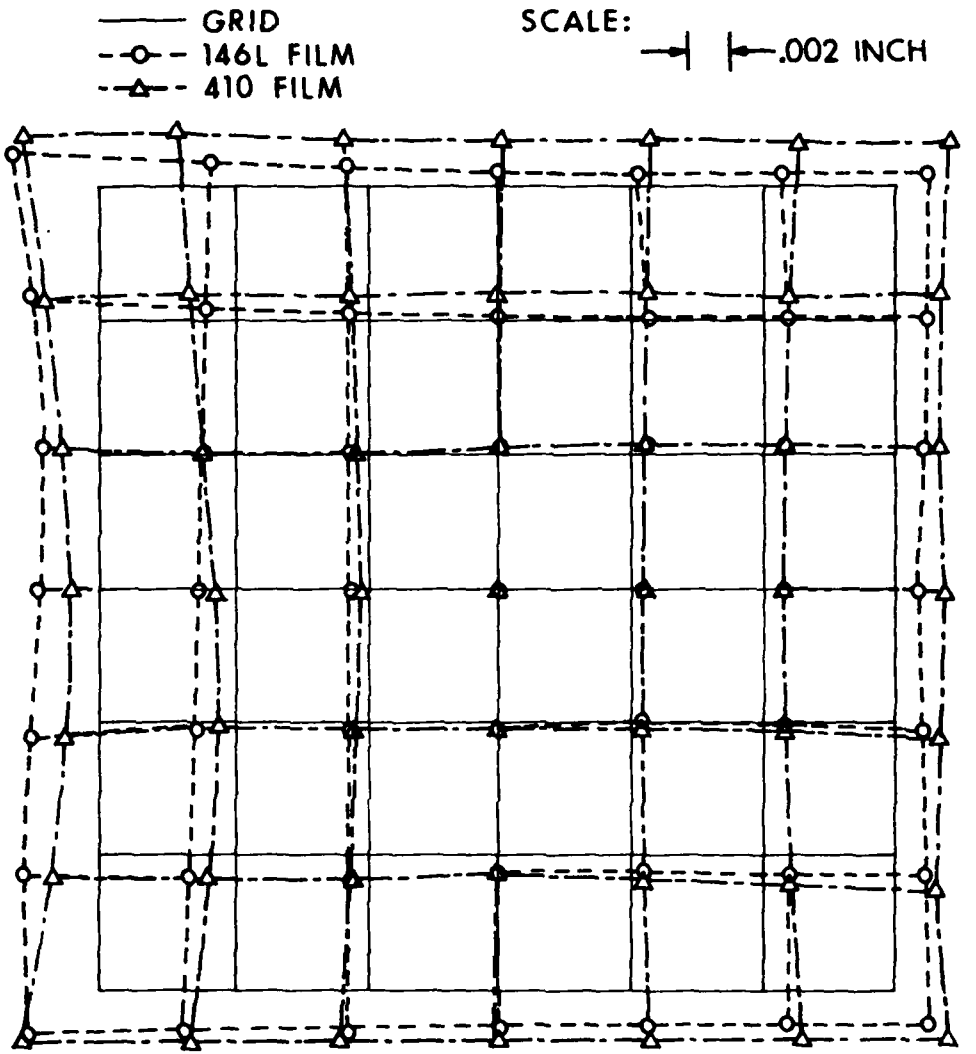

Figure 8. Comparison of Distortion Produced by 410-Film and 146-L Film

as a reference point. However, details at the end of the beam may be poorly defined as a result of the intensity setting, the film exposure, grain clusters, image distortion at etched graticule lines, and local beam distortions which are unexplained. Consequently, it may be impossible to locate this reference point with an uncertainty less than 0.05 mm (approximately 0.2 μs with a sweep time of 150 μs). An RC discharge signal may encounter many of the same problems and frequently cannot be depended upon to provide better accuracy.

E. Operator Error.

An operator must exercise judgment when positioning the crosshair during a record measurement. Judgment produces some inconsistency or error in the measured values. For an evaluation of this error, the transparent copy of a precision grid was measured on an optical comparator, and then immediately remeasured without altering the record alignment. The comparison of measured and remeasured values is presented in Figure 9. This scale does not apply to solid line. An error of from 0.1 μs to 0.2 μs can be attributed to operator judgment. However, it should be noted that the transparent copy of a precision grid provides clear lines surrounded by dense background. This provides the optimum situation for centering the crosshair on the line being measured. Even with this advantage, error between measurement and remeasurement was 0.1 μs to 0.2 μs. This judgment error can be expected to increase when record quality deteriorates or when measurements must be made at the end point of a blanked beam.

F. Comparator Errors.

Polaroid film records are read on an optical comparator. These records are placed on a coordinate measuring stage which is equipped with both optical and digital readouts. The X-Y coordinates of these records are printed on paper tape, and then converted to meaningful quantities. Errors can be imparted to image coordinates by the comparator and these errors depend on the type and construction of the instrument. Measurement biases can arise from temperature which affect the length of the lead screws. Temperature changes can arise from different sources including friction. Young[6] observed comparator error of 0.003 to 0.004 mm in a measured length of 260 mm. The length of an oscilloscope record is usually less than 100 mm, and if Young's observed error can be applied to these records, then error introduced by the comparator is only about 0.001 to 0.002 mm which is essentially negligible.

---

[6] *H. E. M. Young, "Wild STK-1 Stero Comparator Calibration and Coordinate Refinement," MA Sci. Thesis, University of Toronto, 1968.*

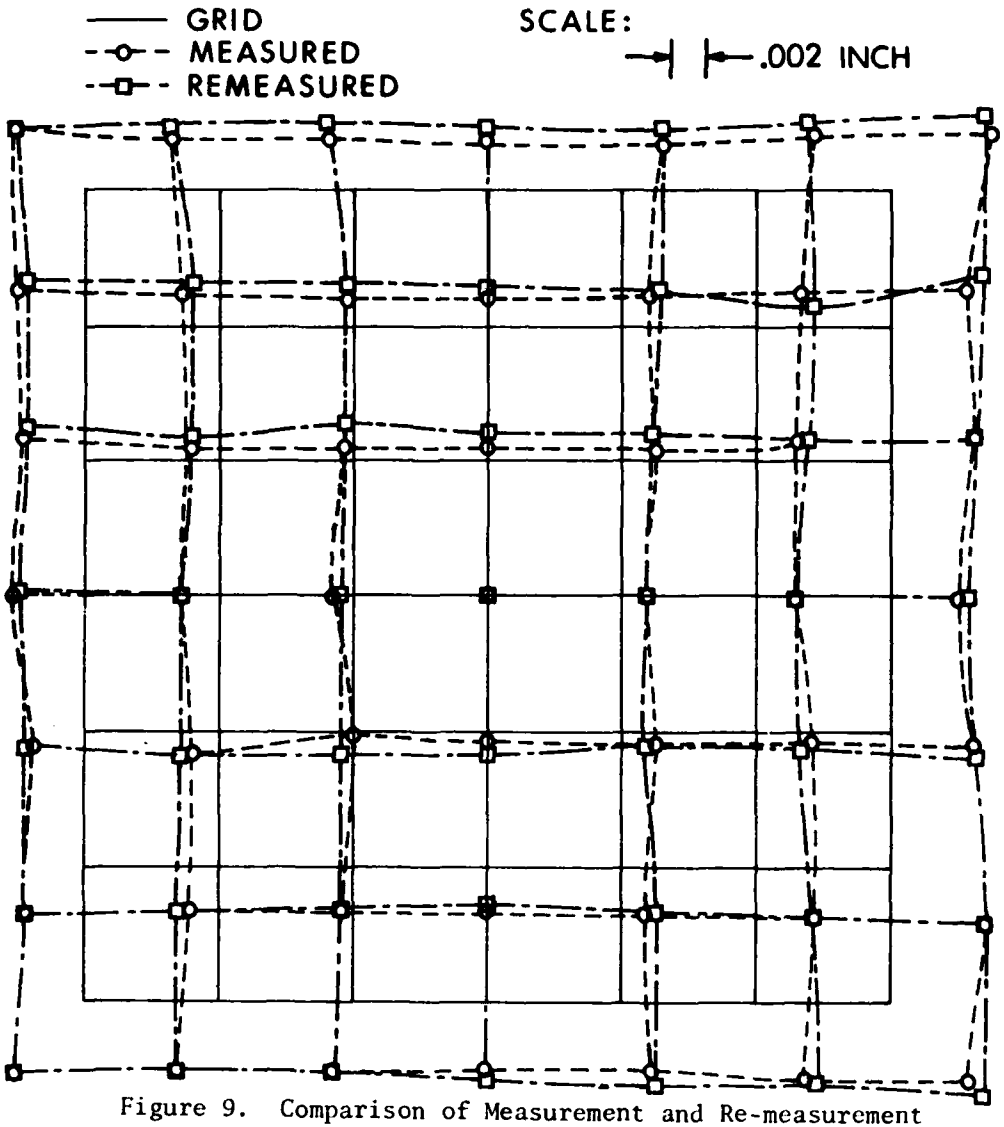

Figure 9. Comparison of Measurement and Re-measurement

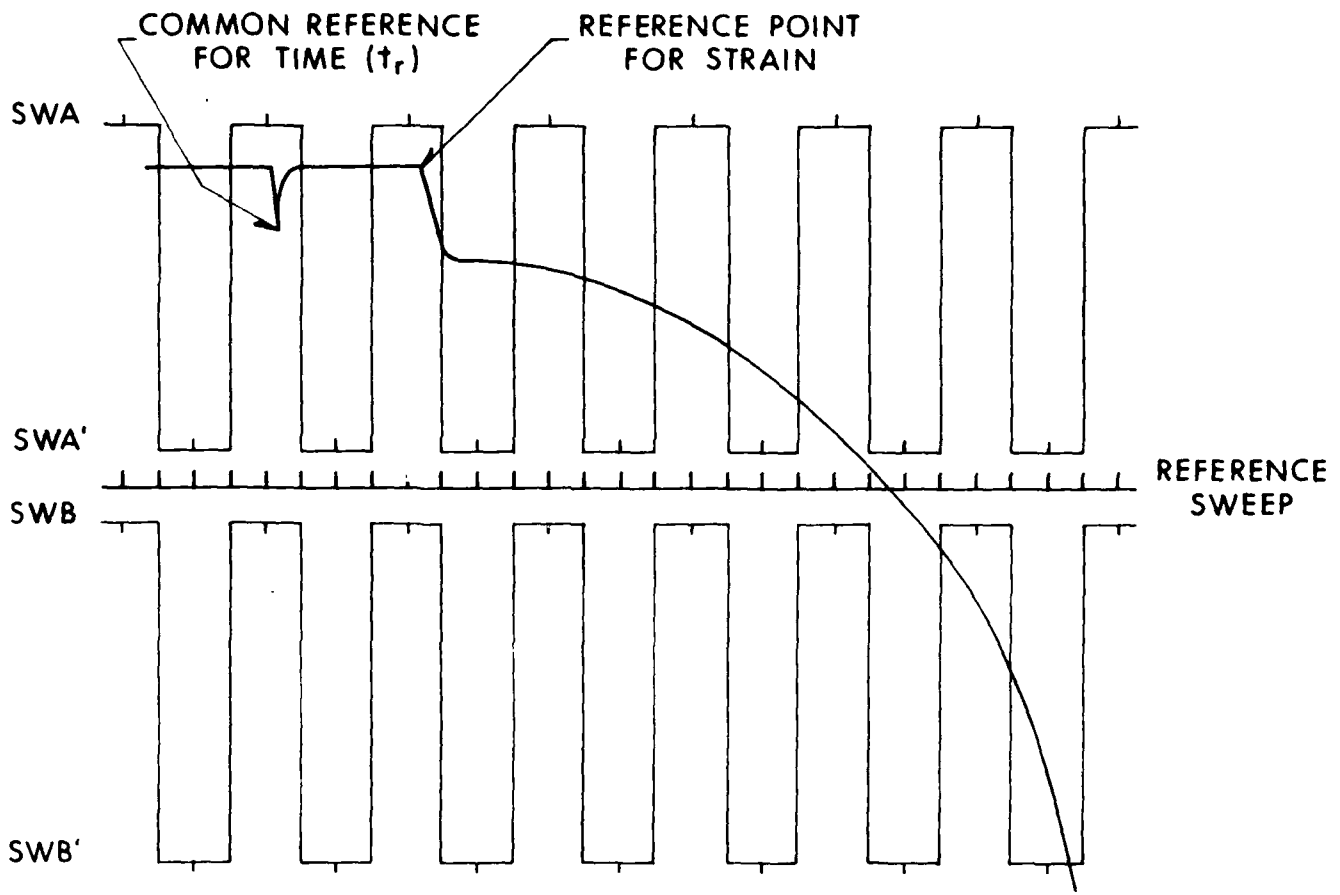

Figure 10. Modified Calibration Procedure

IV. MODIFIED CALIBRATION PROCEDURE

The format of the oscilloscope records in Figure 2 does not permit accurate measurements when records suffer from the distortion shown in Figure 7. However, the record format can be modified to reduce the influence of distortion. All records show that the distortion in the central region is least, so the reference sweep necessary for record alignment can be located in that region where distortion produces minimum curvature. The distortion plot also suggests that the timing error, to a close approximation, increases linearly with distance from the horizontal axis. To evaluate this error, the calibration must establish time as a function of distance along the horizontal axis, and corresponding time as a function of distance at extreme locations above and below the horizontal axis.

Figure 10 shows the calibration format used to determine time from distorted test records. In this format, time marks are superimposed on square waves which are recorded above and below the horizontal axis. Each square wave extends from near the horizontal axis to the extreme off-axis distance where data are recorded. In practice only maxima and minima appear on a photographic record; the writing rate in rising and falling portions of a square wave is too high to produce an exposure. The superimposed time marks occur at five-microsecond intervals, and the period of the square wave is slightly longer than ten microseconds. So each maximum and minimum will always have at least one superimposed time mark. A record is aligned for measurement by using the reference sweep located along the horizontal axis where it is least influenced by distortion. Measurement of the time marks on maxima and minima of the square waves provides the data by which time is determined over the entire record. This measurement shows that time marks located close to the horizontal axis are in close agreement after they are related by a constant time interval. However, it is found that the projection from an axial time mark usually does not pass through the midpoint between off-axis time marks. This timing error depends on the horizontal location, X, and on the distance from the horizontal axis. Referring to Figure 10, it is assumed that the timing error is zero between SWA′ and SWB (because two square waves are very close to each other), is a maximum at both SWA and SWB′, and varies linearly at intermediate off-axis distances. A linear approximation should satisfy the goal of one percent accuracy for the velocity of the faster elastic portion of the stress wave. A parabolic fit should provide a slight improvement.

The calibration data are treated by cubic fits. The position, X, of time marks is related to time, t, by the relationship,

$$t_1 = a_1 + b_1 X + c_1 X^2 + d_1 X^3 \ ,$$

where subscript "1" refers to off-axis location SWA and a_1, b_1, c_1 and d_1 are coefficients of the cubic fit. Similarly, at SWA′

$$t_2 = a_2+b_2X+c_2X^2+d_2X^3 \quad .$$

At corresponding values of X, t_2, and t_1 are usually different. The time at t_1 is $t_2+\Delta t_1$, where Δt_1 is the correction at location SWA. With the distortion shown in Figure 7 the correction, Δt_1, should be positive at early times and negative at late times; it is related to X by the expression,

$$\Delta t_1 = e_1+f_1X+g_1X^2+h_1X^3 \quad .$$

where e_1, f_1, g_1, and h_1 are the coefficients of the cubic fit. Between SWA and SWA´ the correction at an off-axis location, Y, is given by,

$$\Delta t_{2,1} = \Delta t_1 \left(\frac{Y_2-Y}{Y_2-Y_1}\right) \quad ,$$

and the time between SWA and SWA´ is given by

$$t = t_2+ \Delta t_{2,1} \quad .$$

Between SWA´ and SWB, $t = t_2$. At SWB,

$$t_3 = a_3+b_3X+C_3X^2+d_3X^3.$$

The trains of time marks are usually displaced on the two square waves. Consequently, time along SWB is displaced from time along SWA´ by a constant time difference, K. At SWB,

$$t = t_2 = t_3+K \quad .$$

At SWB´,

$$t_4 = a_4+b_4X+c_4X^2+d_4X^3 \quad .$$

Again, at corresponding values of X, t_3 and t_4 are usually different. The time at t_4 is $t_3+\Delta t_4$, where Δt_4 is the correction at SWB´. The correction, Δt_4, is given by the expression,

$$\Delta t_4 = e_4+f_4X+g_4X^2+h_4X^3 \quad ,$$

and between SWB and SWB´ the correction at an off-axis location, Y, is given by,

$$\Delta t_{3,4} = \Delta t_4 \left(\frac{Y-Y_3}{Y_4-Y_3} \right)$$

The time between SWB and SWB´ is then given by

$$t = (t_3+k) + \Delta t_{3,4} = t_2 + \Delta t_{3,4} \quad .$$

Time, t, is established as time along SWA´ or SMB. It is usually necessary for time to be measured from a reference point common to all records. This time, t_{cr}, is given by,

$$t_{cr} = t-t_r,$$

where time, t_r, is at the common reference point indicated in Figure 10.

A worked out example is given below. The coefficients of the cubic fit are calculated at each location.

At SWA

a_1 = -7.239013 b_1 = 0.01906752

c_1 = .2681161E-07 d_1 = .2849293E-11

At SWA´

a_2 = -7.177959 b_2 = 0.01933765

c_2 = -.1000963E-06 d_2 = .149783E-10

At SWB

a_3 = -7.021482 b_3 = 0.01924243

c_3 = -.8452874E-07 d_3 = .1507527E-10

and at SWB´

a_4 = -6.800771 b_4 = 0.01903816

c_4 = .2372174E-07 d_4 = .7440509E-12

The coefficients of the cubic fit that relate the time correction and position, X, of the time marks are also calculated at SWA and at SWB´.

At SWA

e_1 = -.3475977E-03 f_1 = -.3498629E-03

g_1 = .1553328E-06 h_1 = -.1510397E-10

and at SWB;

e_4 = .1266629E-02 f_4 = .8477959E-04

g_4 = .4949229E-08 h_4 = -.3494646E-11

The correction at location SWA and correction between SWA and SWA´ at an off-axis location, Y, are calculated and are given by,

$$\Delta t_1 = -0.1977 \ \mu s$$

$$\Delta t_{2,1} = -0.1294 \ \mu s$$

and the time between SWA and SWA´ is given by

$$t = t_2 + \Delta t_{2,1} = 31.4697 \ \mu s$$

where t_2 is calculated for the coefficients of cubic fit (a_2, b_2, c_2 and d_2) for any X. Similarly, the correction at location SWB´, and correction between SWB and SWB´ at an off-axis location, Y, are calculated and are given by,

$$\Delta t_4 = 0.2034 \ \mu s$$

$$\Delta t_{3,4} = 0.2091 \ \mu s$$

and the time between SWB and SWB´ is given by

$$t = (t_3 + K) + \Delta t_{3,4} = 43.6410 \ \mu s$$

where t_3 is calculated from a_3, b_3, c, and d_3 at any given X, and K is a constant time difference between SWA´ and SWB.

V. CONCLUSIONS

Any significant improvement in the accuracy of data from photographic records has to come through gradual elimination of these various sources of inaccuracies of the image coordinates. There has been an improvement from the use of a modified calibration procedure, but 0.1 μs accuracy is difficult to achieve. Image coordinates are still afflicted by these systematic errors even after the correction. The best solution to these problems may be to replace the analog oscilloscopes by digital recorders which do not require optical devices for recording or reducing test data. With this recording system, the tests records can be stored on magnetic disks. These stored records can be directly transferred to a minicomputer for analytical computations. This system minimizes the handling of test data manually and eliminates the measurement errors.

ACKNOWLEDGEMENT

I would like to express my sincere appreciation to G. E. Hauver for his guidance, valuable advice, and directing the project.

REFERENCES

1. G. E. Hauver, "Penetration with Instrumented Rods," Int. J. Eng. Sci., 16, pp. 871-877, 1978.

2. T. W. Wright, "A Theoretical Framework and Comparison With Instrumented Impacts," 12th Annual Army Science Conference, West Point, NY, 1980.

3. R. E. Franz, "Quasi-Static Stress-Strain Curves, S-7 Tool Steel", Report No. ARBRL-MR-03067, Ballistic Research Laboratory, Aberdeen Proving Ground, MD. (AD #A093773)

4. D. D. Preonas and R. F. Prater, "Quantitative Motion Analysis from Rotating Mirror Framing Camera Records", Journal of the SMPTE, Vol. 79, July 1970.

5. J. Vlcek, "Systematic Errors of Image Coordinates," Photogrammetric Engineerings, Vol. 35, pp. 585-593, 1969.

6. H. E. M. Young, "Wild STK-1 Stereo Comparator Calibration and Coordinate Refinement", MA Sci. Thesis, University of Toronto, 1968.

DISTRIBUTION LIST

No. of Copies	Organization
12	Commander Defense Technical Info Center ATTN: DDC-DDA Cameron Station Alexandria, VA 22314
1	Deputy Assistant Secretary of the Army (R&D) Department of the Army Washington, DC 20310
1	HQDA (DAMA-ARP-P, Dr. Watson) Washington, DC 20310
1	HQDA (DAMA-MS) Washington, DC 20310
1	Commander US Army Ballistic Missile Defense Systems Command ATTN: SENSC, Mr. Davidson P. O. Box 1500 Huntsville, AL 35804
1	Director US Army Advanced BMD Technology Center ATTN: CRDABH-%, W. Loomis P. O. Box 1500, West Station Huntsville, AL 35807
1	Commander US Army War College ATTN: Lib Carlisle Barracks, PA 17013
1	Commander US Army Command and General Staff College ATTN: Archives Fort Leavenworth, KS 66027
1	Commander US Army Materiel Development and Readiness Command ATTN: DRCDMD-ST 5001 Eisenhower Avenue Alexandria, VA 22333
2	Commander US Army Armament Research and Development Command ATTN: DRDAR-TSS (2 cys) Dover, NJ 07801
1	Commander US Army Armament Materiel Readiness Command ATTN: DRSAR-LEP-L, Tech Lib Rock Island, IL 61299
1	Director US Army ARRADCOM Benet Weapons Laboratory ATTN: DRDAR-LCB-TL Watervliet, NY 12189
1	Commander US Army Watervliet Arsenal ATTN: Dr. E. Schneider Watervliet, NY 12189
1	Commander US Army Aviation Research and Development Command ATTN: DRDAV-E 4300 Goodfellow Boulevard St. Louis, MO 63120
1	Director US Army Air Mobility Research and Development Laboratory Ames Research Center Moffett Field, CA 94035
1	Commander US Army Communications Research and Development Command ATTN: DRDCO-PPA-SA Fort Monmouth, NJ 07703
1	Commander US Army Electronics Research and Development Command Technical Support Activity ATTN: DELSD-L Fort Monmouth, NJ 07703

DISTRIBUTION LIST

No. of Copies	Organization
1	Commander US Army Harry Diamond Labs ATTN: DRXDO-TI 2800 Powder Mill Road Adelphi, MD 20783
1	Commander US Army Missile Command ATTN: DRSMI-R Redstone Arsenal, AL 35809
1	Commander US Army Missile Command ATTN: DRSMI-YDL Redstone Arsenal, AL 35809
2	Commander US Army Mobility Equipment Research & Development Command ATTN: DRDME-WC DRDME-RZT Fort Belvoir, VA 22060
1	Commander US Army Natick Research and Development Center ATTN: DRXRE, Dr. D. Sieling Natick, MA 01762
1	Commander US Army Tank Automotive Rsch and Development Command ATTN: DRDTA-UL Warren, MI 48090
1	Commander US Army Electronics Proving Ground ATTN: Tech Lib Fort Huachuca, AZ 85613
3	Commander US Army Materials and Mechanics Research Center ATTN: DRXMR-T, J. Mescall R. Shea S. C. Chou Watertown, MA 02172
1	Commander US Army Research Office P. O. Box 12211 Research Triangle Park NC 27709
1	Director US Army TRADOC Systems Analysis Activity ATTN: ATAA-SL, Tech Lib White Sands Missile Range NM 88002
1	Office of Naval Research Department of the Navy ATTN: Code 402 Washington, DC 20360
1	Commander Naval Surface Weapons Center ATTN: Code GR-9, Dr. W. Soper Dahlgren, VA 22448
1	Commander and Director Naval Electronics Laboratory ATTN: Lib San Diego, CA 92152
3	Commander Naval Research Laboratory ATTN: Code 5270, F. MacDonald Code 2020, Tech Lib Code 7786, J. Baker Washington, DC 20375
1	AFATL (DLDG) Eglin AFB, FL 32542
1	AFATL (DLDL, MAJ J.D. Morgan) Eglin AFB, FL 32542
1	AFATL (DLYW) Eglin AFB, FL 32542
1	RADC (EMTLD, Lib) Griffiss AFB, NY 13440

DISTRIBUTION LIST

No. of Copies	Organization
1	AUL (3T-AUL-60-118) Maxwell AFB, AL 36112
1	AFFDL/FB, Dr. J. Halpin Wright-Patterson AFB, OH 45433
1	IBM Watson Research Center ATTN: R. A. Toupin Poughkeepsie, NY 12601
9	Sandia Laboratories ATTN: Mr. L. Davison Div 5163 Dr. C. Harness H. J. Sutherland Code 5133 Code 1721 Dr. P. Chen L. Berthold W. Herrmann Albuquerque, NM 87115
5	Brown University Division of Engineering ATTN: Prof. R. Clifton Prof. H. Kolsky Prof. A. Pipkin Prof. P. Symonds Prof. J. Martin Providence, RI 02192
4	California Institute of Tech Division of Engineering and Applied Science ATTN: Dr. J. Mikowitz Dr. E. Sternberg Dr. J. Knowles Dr. T. Coguhey Pasadena, CA 91102
1	California Research and Technology, Inc. ATTN: Dr. D. L. Orphal 4049 First Street, Suite 135 Livermore, CA 94550
4	Carnegie Mellon University Department of Mathematics ATTN: Dr. D. Owen Dr. M. E. Gurtin Dr. B. Coleman Dr. W. Williams Pittsburgh, PA 15213
2	Catholic University of America School of Engineering and Architecture ATTN: Prof. A. Durelli Prof. J. McCoy Washington, DC 20017
1	Harvard University Division of Engineering and Applied Physics ATTN: Dr. G. Carrier Cambridge, MA 02138
2	Iowa State University Engineering Research Lab ATTN: Dr. G. Nariboli Dr. A. Sedov Ames, IA 50010
1	Johns Hopkins University ATTN: Prof. J. Bell 34th and Charles Streets Baltimore, MD 21218
6	Johns Hopkins University Applied Physics Lab ATTN: Dr. E. P. Gray Dr. R. E. Gorozdos Dr. B. F. Kim Dr. K. A. Patocki Dr. E. P. Cunnighan Dr. R. Weiss Laurel, MD 20810
2	Lehigh University Center for the Application of Mathematics ATTN: Dr. E. Varley Dr. R. Rivlin Bethlehem, PA 18015

DISTRIBUTION LIST

No. of Copies	Organization
1	Massachusetts Institute of Tech ATTN: Dr. R. Probstein 77 Massachusetts Avenue Cambridge, MA 02139
1	Michigan State University College of Engineering ATTN: Prof. W. Sharpe East Lansing, MI 48823
1	New York University Department of Mathematics ATTN: Dr. J. Keller University Heights New York, NY 10053
1	North Carolina State University Dept of Engineering Mechanics ATTN: Dr. W. Bingham P. O. Box 5071 Raleigh, NC 27607
1	Pennsylvania State University Engineering Mechanical Dept. ATTN: Prof. N. Davids University Park, PA 16502
2	Forrestal Research Center Aeronautical Engineering Lab Princeton University ATTN: Dr. S. Lam Dr. A. Eringen Princeton, NJ 08540
1	Purdue University Institute for Mathematical Sciences ATTN: Dr. E. Cumberbatch Lafayette, IN 47907
2	Rice University ATTN: Dr. R. Bowen Dr. C. C. Wang P. O. Box 1892 Houston, TX 77001
1	Southern Methodist University Solid Mechanics Division ATTN: Prof. H. Watson Dallas, TX 75221
2	Southwest Research Institute Dept of Mechanical Sciences ATTN: Dr. U. Kingholm Dr. W. Baker 8500 Culebra Road San Antonio, TX 78228
3	SRI International ATTN: D. Curran L. Seaman Y. Gupta Menlo Park, CA 94025
1	Temple University College of Engineering Tech ATTN: Dr. R. M. Haythornthwaite Dean Philadelphia, PA 19122
1	Tulane University Dept of Mechanical Engineering ATTN: Dr. S. Cowin New Orleans, LA 70112
2	University of California ATTN: Dr. M. Carroll Dr. P. Naghdi Berkeley, CA 94704
1	University of California Dept of Aerospace and Mechanical Engineering Science ATTN: Dr. Y. C. Fung P. O. Box 109 La Jolla, CA 92037
1	University of California Department of Mechanics ATTN: Dr. R. Stern 504 Hilgard Avenue Los Angeles, CA 90024

DISTRIBUTION LIST

No. of Copies	Organization
1	University of California at Los Angeles Department of Mechanics ATTN: W. Goldsmith Los Angeles, CA 90024
1	University of Delaware Dept of Mechanical Engineering ATTN: Prof. J. Vinson Prof. Chou Prof. Danberg Newark, DE 19711
2	University of Houston Dept of Mechanical Engineering ATTN: Dr. T. Wheeler Dr. R. Nachlinger Houston, TX 77004
1	University of Illinois Department of Theoretical and Applied Mechanics ATTN: Dr. D. Carlson Urbana, IL 61801
2	University of Illinois at Chicago Circle College of Engineering Dept of Materials Engineering ATTN: Prof. A. Schultz Dr. T. C. T. Ting P. O. Box 4348 Chicago, IL 60680
1	University of Iowa ATTN: Dr. L. Valanis Iowa City, IA 52240
4	University of Kentucky Dept of Engineering Mechanics ATTN: Dr. M. Beatty Prof. O. Dillon, Jr. Prof. P. Gillis Dr. D. Leigh Lexington, KY 40506
2	The University of Maryland Dept of Mechanical Engineering ATTN: Prof. J. Yang Dr. J. Dally College Park, MD 20742
1	University of Minnesota Dept of Engineering Mechanics ATTN: Dr. R. Fosdick Minneapolis, NN 55455
1	University of Notre Dame Department of Metallurgical Engineering & Materials Sciences ATTN: Dr. N. Fiore Notre Dame, IN 46556
1	University of Pennsylvania Towne School of Civil and Mechanical Engineering ATTN: Prof. Z. Hashin Philadelphia, PA 19105
3	University of Texas Dept of Engineering Mechanics ATTN: Dr. M. Stern Dr. M. Bedford Prof. Ripperger Austin, TX 78712
1	University of Washington Dept of Mechanical Engineering ATTN: Prof. J. Chalupnik Seattle, WA 98105
2	Yale University ATTN: Dr. B. Chu Dr. E. Onat 400 Temple Street New Haven, CT 96520

DISTRIBUTION LIST

Aberdeen Proving Ground

Dir, USAMSAA
ATTN: DRXSY-D
DRXSY-MP, H. Cohen
Cdr, USATECOM
ATTN: DRSTE-TO-F
Dir, USACSL, Bldg. E3516, EA
ATTN: DRDAR-CLB-PA
Dir, USACSL, Bldg. E3330, EA
ATTN: Dr. E. Poziomek
Mr. E. Crumb
Mr. R. Kipp

USER EVALUATION OF REPORT

Please take a few minutes to answer the questions below; tear out this sheet, fold as indicated, staple or tape closed, and place in the mail. Your comments will provide us with information for improving future reports.

1. BRL Report Number _____

2. Does this report satisfy a need? (Comment on purpose, related project, or other area of interest for which report will be used.)

_____

_____

_____

3. How, specifically, is the report being used? (Information source, design data or procedure, management procedure, source of ideas, etc.) _____

_____

_____

4. Has the information in this report led to any quantitative savings as far as man-hours/contract dollars saved, operating costs avoided, efficiencies achieved, etc.? If so, please elaborate.

_____

_____

5. General Comments (Indicate what you think should be changed to make this report and future reports of this type more responsive to your needs, more usable, improve readability, etc.) _____

_____

_____

_____

6. If you would like to be contacted by the personnel who prepared this report to raise specific questions or discuss the topic, please fill in the following information.

Name: _____

Telephone Number: _____

Organization Address: _____

_____

_____

FOLD HERE

Director
US Army Ballistic Research Laboratory
Aberdeen Proving Ground, MD 21005

NO POSTAGE
NECESSARY
IF MAILED
IN THE
UNITED STATES

OFFICIAL BUSINESS
PENALTY FOR PRIVATE USE. $300

BUSINESS REPLY MAIL
FIRST CLASS PERMIT NO 12062 WASHINGTON, DC
POSTAGE WILL BE PAID BY DEPARTMENT OF THE ARMY

Director
US Army Ballistic Research Laboratory
ATTN: DRDAR-TSB
Aberdeen Proving Ground, MD 21005

FOLD HERE